Vignetting in PFM1 High Resolution Interferograms

David Naylor, Trevor Fulton, Peter Davis

Version 0.4

20 April 2005

Introduction

The purpose of this document is to present the first results of the analysis of the vignetting observed in the high-resolution interferogram data taken during the SPIRE PFM1 test campaign and, in particular, to investigate the relationship between BDA pixel location and vignetting. This work is intended to complement the analysis undertaken by Marc Ferlet.

This preliminary analysis focussed on the subset of the PFM1 data where a high-resolution interferogram was measured and where the cold blackbody (CBB) was the primary source. There are four datasets that fit these conditions, details of which are given in the table below.

Scan Time[hh:mm:ss] UTC		Scan Limits [mm]			Iterations	Input ports
Start	End	Start	End	Distance		
20:38:00	20:59:00	4.86	39.26	34.40	16	CBB @ 6.5K
17:34:00	17:54:00	4.88	39.00	34.12	16	CBB @ 9.5K
18:09:00	18:36:00	4.86	39.26	34.40	16	CBB @ 11.5K
19:46:00	19:56:00	4.86	39.26	34.40	4	CBB @ 13K

The method used to calculate the amount of vignetting is described below:

1. The recorded detector signals were interpolated onto evenly spaced position grids (using the interpolated SMEC positions) to create an interferogram.
2. For each CBB temperature scan set, the scans were averaged to increase the signal to noise ratio. As the precise values needed to correct for hysteresis between forward and reverse scans were not known at the time of the analysis, the forward and reverse scans have been averaged separately.
3. The difference between the averaged interferograms corresponding to the 13 K and 6.5 K observations yield an interferogram whose slowly decreasing dc level gives directly the change in modulation efficiency arising from vignetting (or other possible forms of apodization). By taking differences, systematic contributions to the dc signal (detector bias/gain, electronic offset etc) are removed. In this analysis it is assumed that these systematic terms do not vary between different CBB scans for a given pixel.
4. The difference interferograms were then normalized such that their value at zero optical path difference was unity.

Plots of the normalized difference interferograms are shown in the figures below. For the figures below, the CBB temperatures were 13K and 6.5K. Normalized interferograms were calculated for the other possible CBB combinations (13K-11K, 13K-9.5K, etc.); as expected the results were essentially identical. For completeness the corresponding data are shown in Figs 6 – 10 of the appendix.

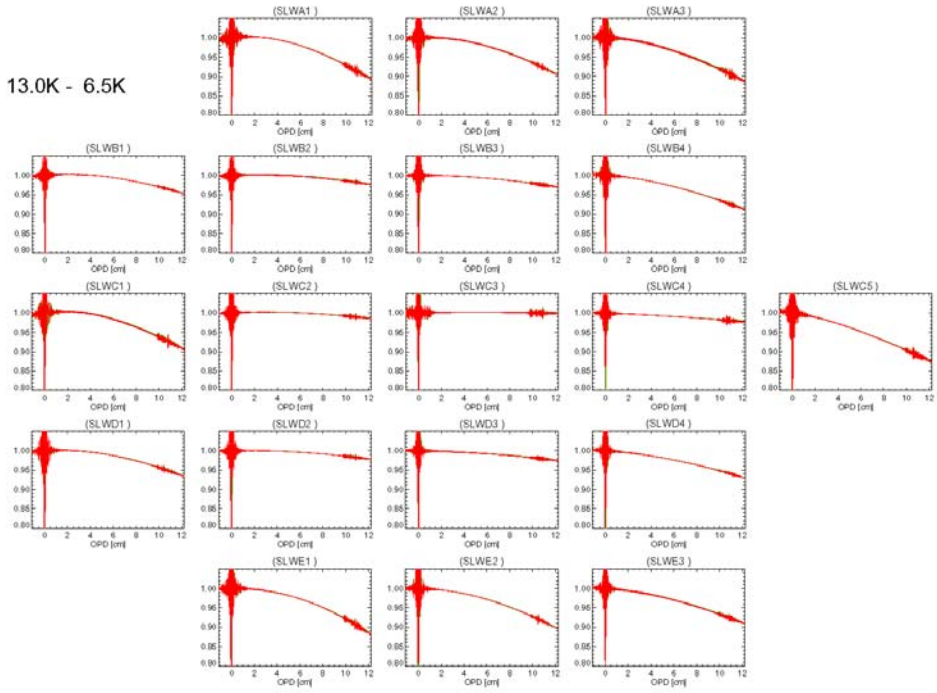

Figure 1: Normalized Difference Interferograms as a function of Optical Path Difference, SLW array. For the plots shown the CBB temperatures were 13K and 6.5K. The **green** curves are the differences between the forward scans; the **red** curves are the differences between the reverse scans.

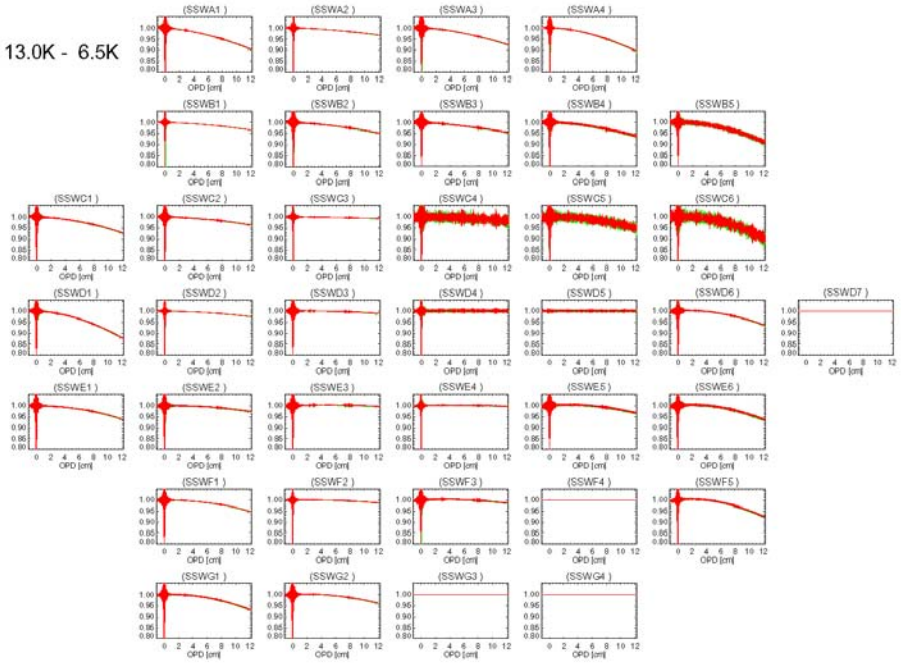

Figure 2: Normalized Difference Interferograms as a function of Optical Path Difference, SSW array. For the plots shown the CBB temperatures were 13K and 6.5K. The **green** curves are the differences between the forward scans; the **red** curves are the differences between the reverse scans.

The same data are presented in Fig 4 in a form that allows direct comparison with the vignetting results of Marc Ferlet's model In Marc's analysis (reproduced in Fig. 3) normalized vignetting is calculated for the central pixel and four field positions at the edge of the spectrometer field of view.

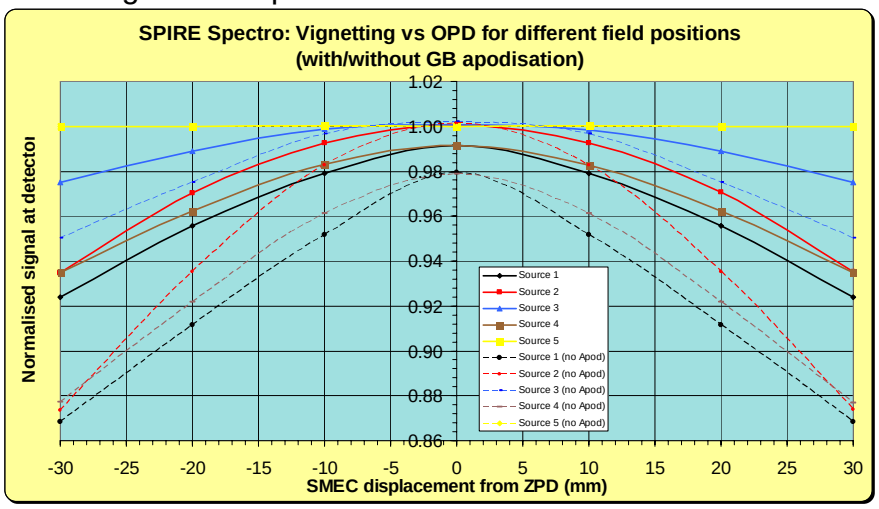

Figure 3: Modelled Vignetting as a function of SMEC Displacement[1].

[1] Ferlet, Marc, *SPIRE PFM1 Testing: Spectrometer issue v0.2*, RAL/SSTD, 15 April 2005

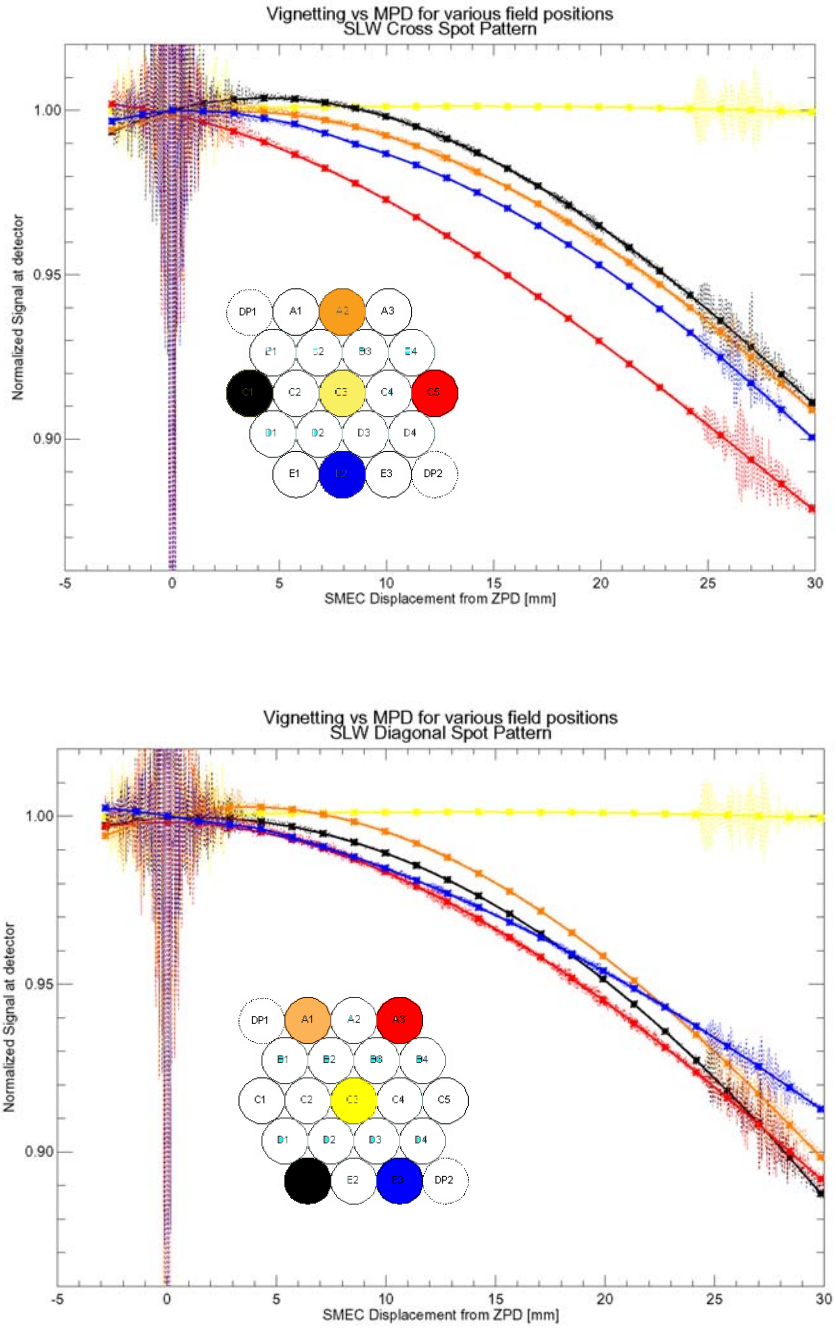

Figure 4: Normalized Difference Interferograms as a function of SMEC Displacement, SLW array. A selection of pixels intended to correspond with the modelled regions. The upper panel corresponds to the vertical cross pattern; the lower panel corresponds to the diagonal cross pattern.

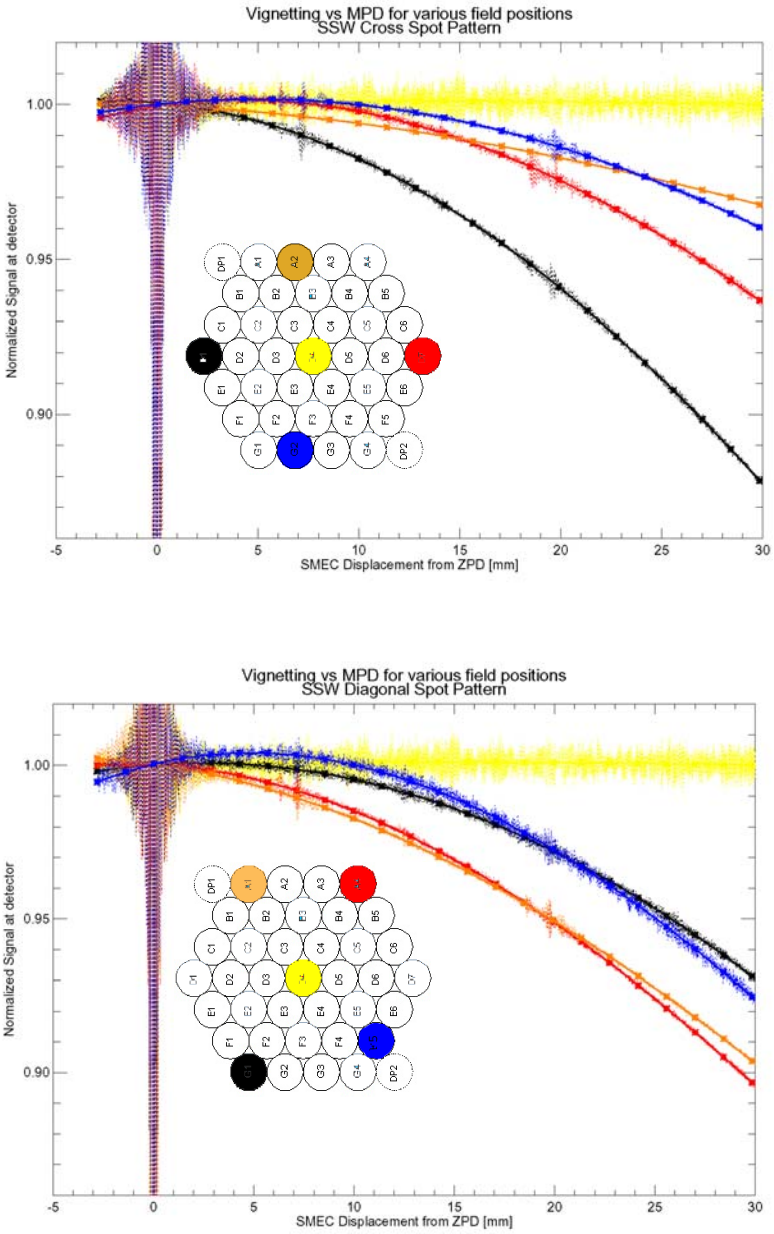

Figure 5: Normalized Difference Interferograms as a function of SMEC Displacement, SSW array. A selection of pixels intended to correspond with the modelled regions. The upper panel corresponds to the vertical cross pattern; the lower panel corresponds to the diagonal cross pattern.

Conclusions

- first results show that the the amount of vignetting is close to that predicted by Marc's model.

- as expected the central pixel shows the least vignetting (essentially only natural apodization) while the effects of vignetting increase as a function of the pixel's off-axis angle.

- it should be a relatively easy matter to determine experimentally, and thus to be able to correct (through applying a variable gain as a function of opd) for the effects of apodization due to vignetting.

- There is some indication of a peak in the normalized vignetting curve for some pixels around 6 mm mechanical path difference. It would be interesting to know if this was due to the focal length of the field lens which is not matched to the location of the zpd pupil image. We have tried to determine the optimum opd pupil image corresponding to the existing field lens, but lack sufficient details of the optical design to see if this might explain the displaced peak. (In any event the pupil within an FTS is always moving due to the changing path difference as the interferometer scans.)

Appendix

Vignetting Observed For Other Temperature Differences

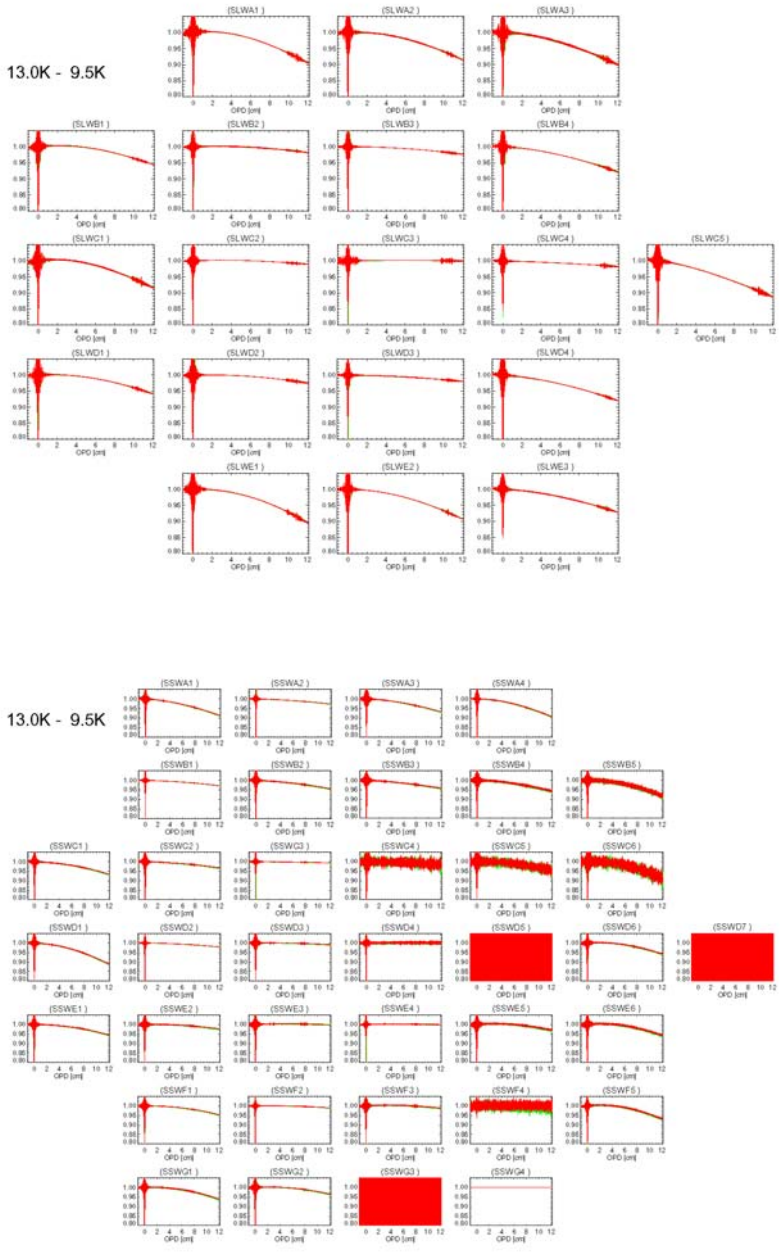

Figure 6 Normalized Difference Interferograms as a function of Optical Path Difference. The upper panel is the SLW array; the lower panel is the SSW array. For the plots shown the CBB temperatures were 13K and 9.5K. The **green** curves are the differences between the forward scans; the **red** curves are the differences between the reverse scans.

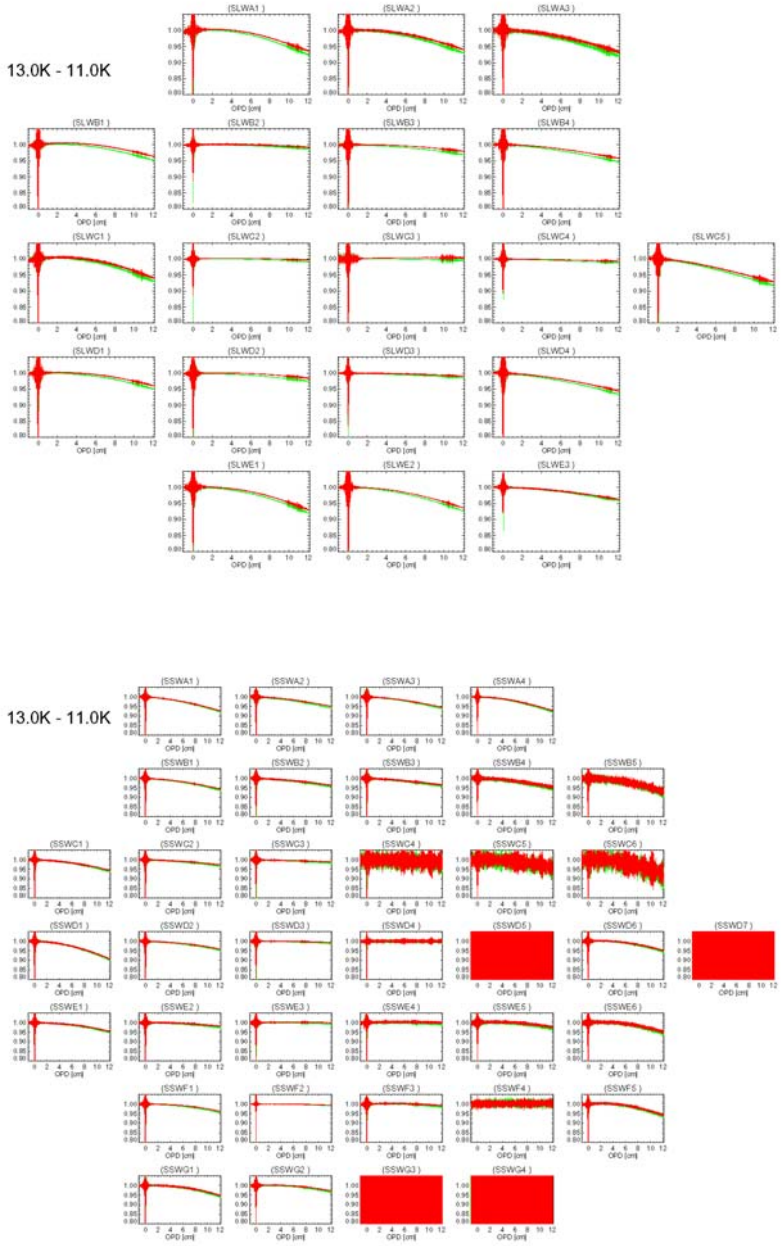

Figure 7 Normalized Difference Interferograms as a function of Optical Path Difference. The upper panel is the SLW array; the lower panel is the SSW array. For the plots shown the CBB temperatures were 13K and 11K. The **green** curves are the differences between the forward scans; the **red** curves are the differences between the reverse scans.

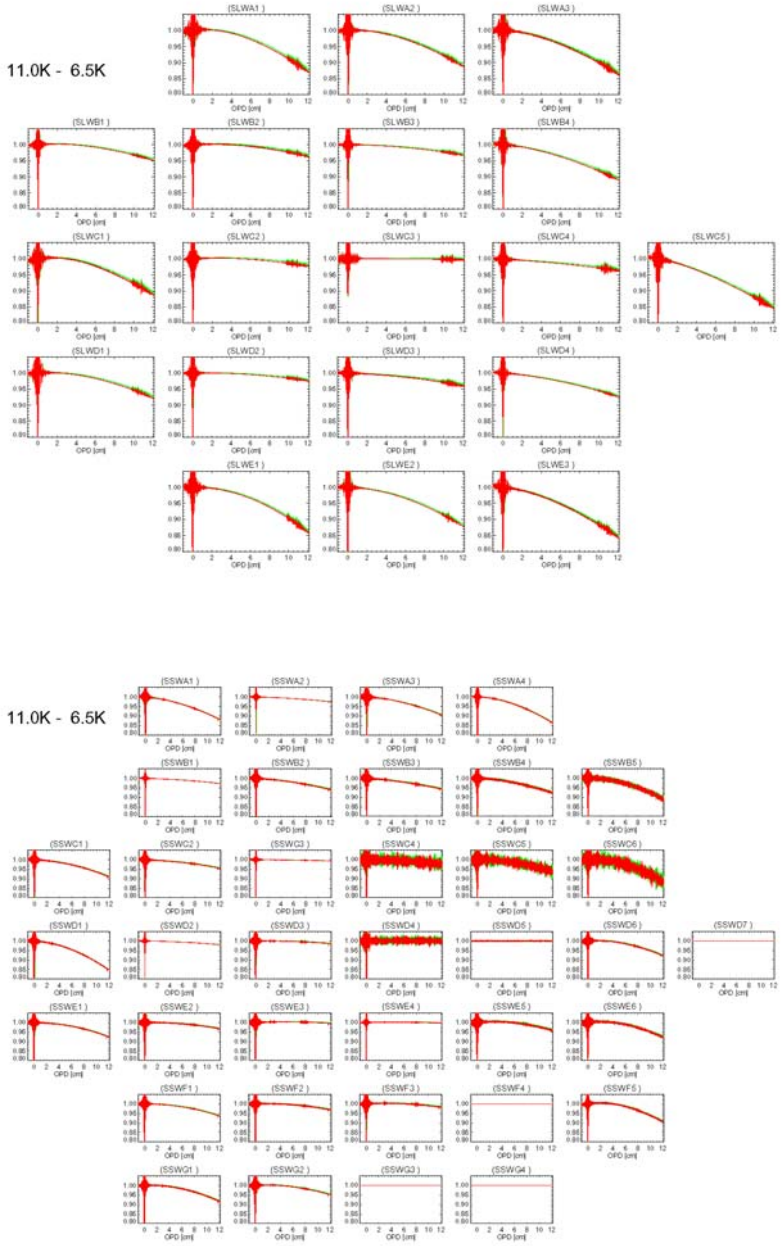

Figure 8 Normalized Difference Interferograms as a function of Optical Path Difference. The upper panel is the SLW array; the lower panel is the SSW array. For the plots shown the CBB temperatures were 11K and 6.5K. The **green** curves are the differences between the forward scans; the **red** curves are the differences between the reverse scans.

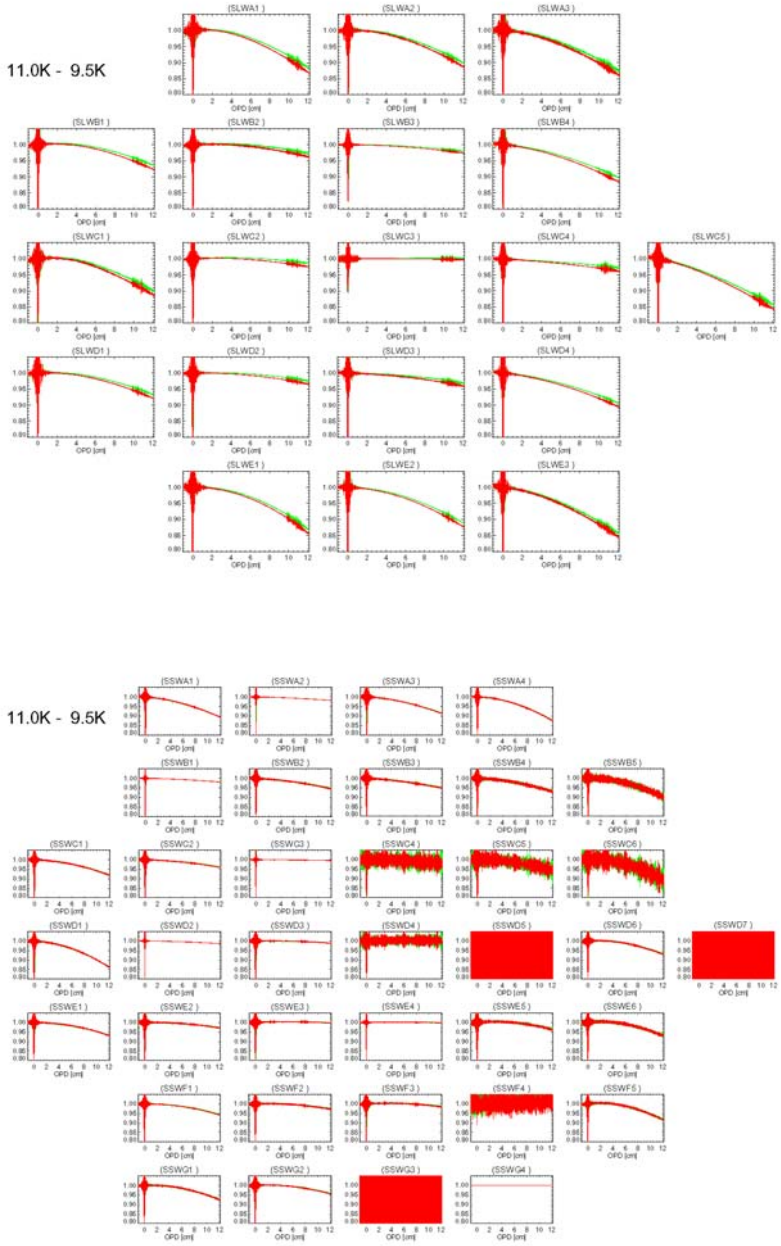

Figure 9 Normalized Difference Interferograms as a function of Optical Path Difference. The upper panel is the SLW array; the lower panel is the SSW array. For the plots shown the CBB temperatures were 11K and 9.5K. The **green** curves are the differences between the forward scans; the **red** curves are the differences between the reverse scans.

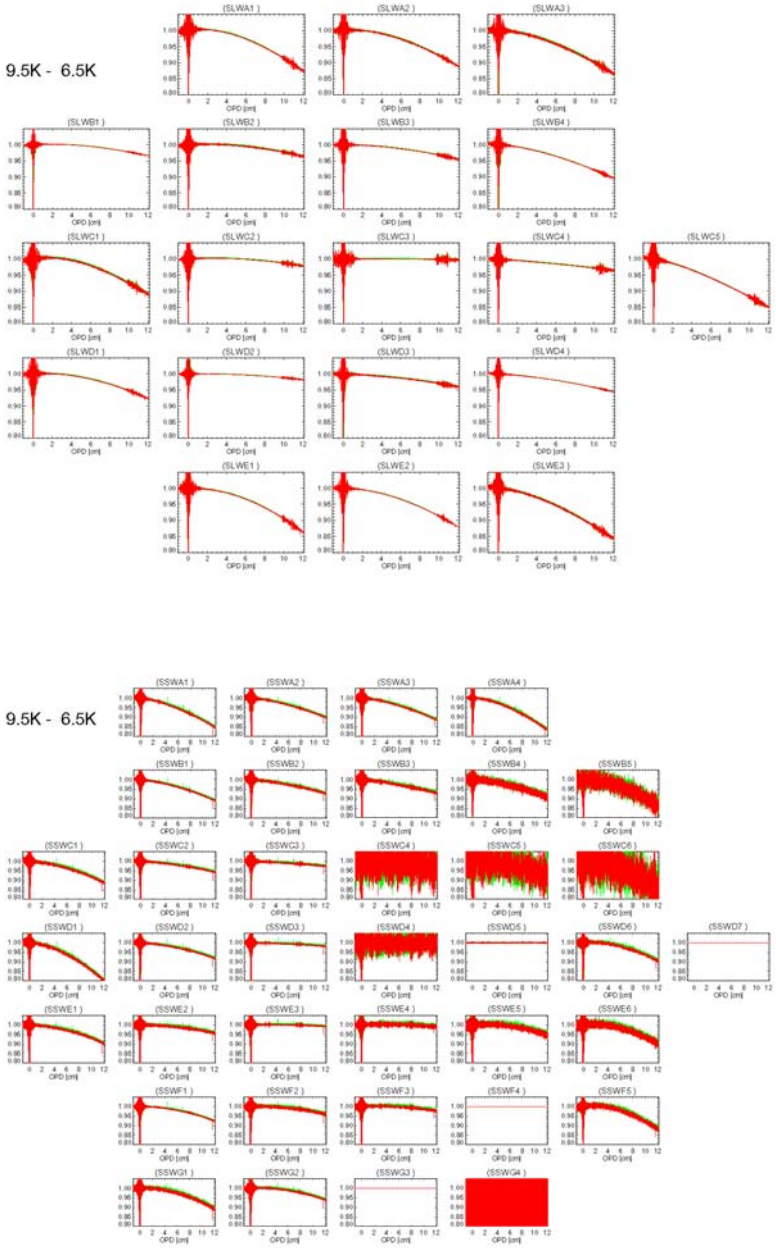

Figure 10 Normalized Difference Interferograms as a function of Optical Path Difference. The upper panel is the SLW array; the lower panel is the SSW array. For the plots shown the CBB temperatures were 9.5K and 6.5K. The **green** curves are the differences between the forward scans; the **red** curves are the differences between the reverse scans.